

## Visualizing the Strain Field in Semiflexible Polymer Networks: Strain Fluctuations and Nonlinear Rheology of *F*-Actin Gels

J. Liu,<sup>1</sup> G. H. Koenderink,<sup>1,\*</sup> K. E. Kasza,<sup>1</sup> F. C. MacKintosh,<sup>2</sup> and D. A. Weitz<sup>1</sup>

<sup>1</sup>*Department of Physics & SEAS, Harvard University, Cambridge, Massachusetts 02138, USA*

<sup>2</sup>*Department of Physics and Astronomy, Vrije Universiteit, Amsterdam, The Netherlands*

(Received 4 October 2006; published 10 May 2007)

We image semiflexible polymer networks under shear at the micrometer scale. By tracking embedded probe particles, we determine the local strain field, and directly measure its uniformity, or degree of affineness, on scales of 2–100  $\mu\text{m}$ . The degree of nonaffine strain depends upon the polymer length and cross-link density, consistent with theoretical predictions. We also find a direct correspondence between the uniformity of the microscale strain and the nonlinear elasticity of the networks in the bulk.

DOI: [10.1103/PhysRevLett.98.198304](https://doi.org/10.1103/PhysRevLett.98.198304)

PACS numbers: 83.60.Df, 83.80.Rs, 87.15.La, 87.16.Ka

Actin is an abundant protein found in eukaryotic cells. *In vitro*, actin can polymerize to form semiflexible filaments (*F*-actin). A myriad of actin binding proteins can both cross-link and bundle these filaments, resulting in an elastic network. Cross-linked *F*-actin networks are an excellent model system with which to study the physics of semiflexible polymer networks; they can also provide insight into the mechanical properties of the cell. These networks exhibit remarkable mechanical behavior. Unlike conventional polymer gels, they are highly elastic even for small volume fractions of protein. Moreover, their elasticity can be highly nonlinear: For highly cross-linked networks, the elasticity exhibits a striking increase in stiffness with strain [1–3]; by contrast, for weakly cross-linked networks the elasticity exhibits a decrease in stiffness with strain on long time scales [4]. Understanding the origin of this behavior remains an important challenge. Several models for the microscopic origin of this nonlinear elasticity have been proposed [3,5,6]. Densely cross-linked networks are predicted to deform affinely, or uniformly, throughout the sample [7–9]; then network stiffening results from entropic stretching of individual semiflexible filaments [1,3,5,10]. By contrast, weakly cross-linked networks are predicted to deform nonaffinely, with a response dominated by bending of individual filaments [7–9,11] which is not expected to lead to strain stiffening [1]. Thus, a critical parameter to test existing models of nonlinear elasticity is the degree to which the network deforms nonaffinely. Experimental measures of this require imaging the network strain field [12], and quantitatively analyzing the degree of nonaffinity.

In this Letter, we directly image the microscale strain field of sheared *F*-actin networks and measure the resulting nonaffinity [13]. Network deformation becomes more affine at higher cross-link density or longer filament length, which correlates directly with the simultaneous appearance of nonlinear elasticity of these networks.

To form *F*-actin networks and to control their structure and connectivity, we use the cross-link scruin [1,14]. Scruin decorates the actin filaments and scruin-scruin in-

teractions lead to the cross-linking, and, at higher concentrations, some filament bundling [15,16]. The scruin cross-links are both rigid and irreversible, ensuring that the network response reflects that of the actin filaments alone [1,10,17]. Furthermore, at low enough scruin concentration, it has been shown that the resulting networks are homogeneous, making this a good model system for our study. We vary the degree of cross-linking by altering the molar ratio of scruin to actin concentrations,  $R = c_S/c_A$ . In addition, the average contour length of *F*-actin,  $L$ , is regulated through addition of the actin severing and capping protein, gelsolin [2,18].

We purify scruin from the acrosomal process of the *Limulus* sperm [19,20]. We gently mix monomeric actin, scruin, gelsolin, and 10x *F*-buffer (20 mM Tris HCl, 20 mM MgCl<sub>2</sub>, 1 M KCl, 2 mM DTT, 2 mM CaCl<sub>2</sub>, 5 mM ATP, pH 7.5) at 4 °C, and add fluorescent carboxylate-modified latex particles of radius 0.5  $\mu\text{m}$  as probes. The solution is loaded immediately into the shear cell, surrounded by mineral oil to prevent drying, and incubated for 1 h at 25 °C. Confocal imaging confirms that all samples are homogeneous networks without bundles [21].

We use an optical shear cell mounted on a confocal microscope (Zeiss LSM 510-Meta), enabling 3D visualization of a sample. The sample is sheared between a fixed top plate, 6 mm in diameter, and a movable microscope cover slip, as shown in the inset of Fig. 1. The gap is  $\sim 100 \mu\text{m}$  and the plates are parallel to within 1  $\mu\text{m}$  over the shear zone. A piezoelectric actuator moves the bottom cover slip up to 30  $\mu\text{m}$ , resulting in strains of at most 30%. For larger strains, we use a cell whose top plate is moved by a micrometer. We find empirically that coating both plates with bovine serum albumin prevents slipping at the surface. At each applied strain, we first collect several images of a single plane and confirm there is no slip or drift. We then collect a  $z$  stack of 121 frames, each separated by 300 nm. We determine the 3D positions of the centers of the  $\sim 200$  particles in the sample, and monitor each of their trajectories [18,22], with a resolution of

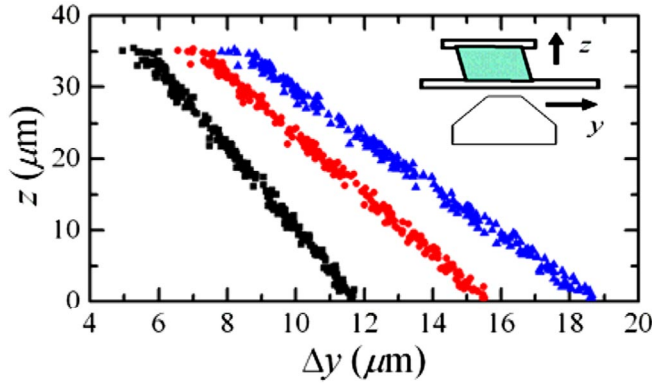


FIG. 1 (color online). Particle position  $y$  at height  $z$ , showing displacement in the shear direction for a typical sample. Different symbols represent different strain amplitudes. The inset shows a schematic of the setup. A shear cell consisting of a fixed top plate and a movable bottom plate is mounted on an inverted microscope.

$\sim 0.02\text{--}0.1\ \mu\text{m}$ , depending on network stiffness, and limited by thermal motion. The particle displacement in the shear direction,  $\Delta y$ , is linear with height,  $z$ , as shown in Fig. 1, where different symbols represent different shear-strain amplitudes. This confirms that the average strain is affine, enabling us to determine the strain applied to the sample,  $\gamma$ , from a fit for each data set.

To measure the rheology of  $F$ -actin networks *in situ*, while the sample is prestressed by an applied  $\gamma$ , we use two-particle (2P) microrheology, which probes the elastic response using correlated motion of pairs of particles; this is a robust technique particularly suitable for actin networks [18]. Because the sample is prestressed, this corresponds to measuring the differential modulus,  $K = d\sigma/d\gamma$ , where  $\sigma$  is stress. For comparison, we also measure both elastic ( $K'$ ) and viscous ( $K''$ ) components using a stress controlled rheometer (Bohlin CVOR) with a parallel-plate geometry using a  $50\text{-}\mu\text{m}$  gap. We superpose a small, oscillatory stress on a static prestress,  $\sigma_0$ , and measure the resultant oscillatory strain to determine  $K'$  and  $K''$  [1,10,23].

The nonlinear rheology of  $F$ -actin networks is critically dependent on the degree of cross-linking [1]. For a highly cross-linked network ( $c_A = 1\ \text{mg/ml}$ ,  $R = 0.06$ ), the viscoelasticity probed by microrheology at all applied  $\gamma$ 's is dominated by a nearly frequency-independent  $K'$  whose magnitude increases with increasing  $\gamma$ , as shown by the lines in Fig. 2(a). We can directly match these data to bulk measurements of  $K'$  by applying increasing values of  $\sigma_0$ , as shown by the symbols in Fig. 2(a). However, even at  $\gamma = 0$ , the microrheology sample corresponds to  $\sigma_0 = 0.3\ \text{Pa}$  (squares). We speculate that this results from the induced strain on the polymerizing sample as the top plate of the shear cell is lowered into position. However, the incremental strains required to increase the applied stress on the bulk sample are identical to those applied to the microrheology sample. By contrast, for a more weakly

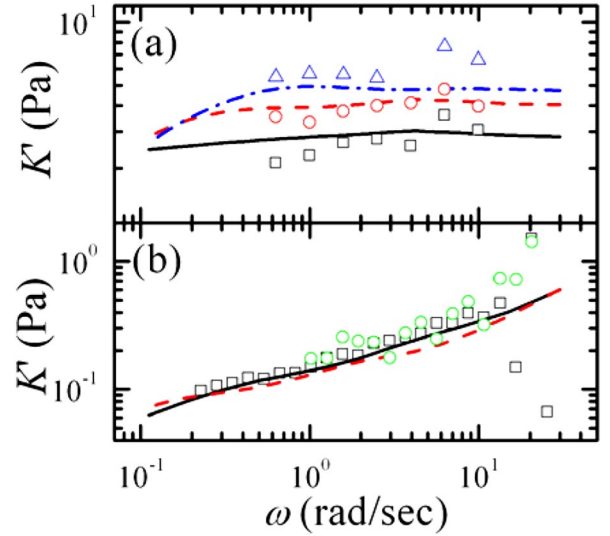


FIG. 2 (color online). (a) For a strongly cross-linked network ( $c_A = 1\ \text{mg/ml}$ ,  $R = 0.06$ ), the  $K'$  measured by 2P microrheology (lines) at different  $\gamma$  (solid line: 0%; dashed line: 15%; dash-dotted line: 24%) is compared with that measured by bulk rheology (symbols) at different  $\sigma_0$  (squares: 0.3 Pa; circles: 0.5 Pa; triangles: 0.75 Pa). (b) For a weakly cross-linked network ( $c_A = 0.5\ \text{mg/ml}$ ,  $R = 0.002$ ), the  $K'$  measured by 2P microrheology (lines) at different  $\gamma$  (solid line: 0%; dashed line: 36%) is compared with that measured by bulk rheology (symbols) at different  $\sigma_0$  (squares: 0; circles: 0.02 Pa). All data are taken at  $25^\circ\text{C}$ .

cross-linked network ( $c_A = 0.5\ \text{mg/ml}$ ,  $R = 0.002$ ),  $K'$  probed by microrheology becomes dominant only at low frequencies and increases with frequency, but is independent of applied  $\gamma$ , up to 36%, as shown by the lines in Fig. 2(b). Identical results, independent of applied stress, are again obtained using bulk rheology, as shown by the symbols in Fig. 2(b).

To probe the microscopic deformation, we compare the relative positions of pairs of particles before and after shear. We show this schematically for two particles separated by distance  $r$  in the inset of Fig. 3(a). The solid line represents the actual separation vector between the particles after the strain is applied while the dashed line represents this separation vector if their motion had been strictly affine. The deviation is characterized by the angle  $\Delta\theta$ , and a corresponding distance,  $r\Delta\theta$ . We define the degree of nonaffinity at a length scale  $r$  as  $N(r) = \langle r^2 \Delta\theta^2 \rangle_r / \gamma^2$ , where we average over all pairs of particles separated by  $r$ . This is equivalent to the method used in Ref. [7], except that our normalization is more sensitive to small changes in  $\Delta\theta$ .

For all samples, we find that  $N(r)$  is independent of the applied strain. Given the normalization of  $N(r)$ , this means that the amplitude of nonaffine deformation is linear in  $\gamma$ . For example, for a highly cross-linked sample ( $c_A = 1\ \text{mg/ml}$ ,  $R = 0.06$ ),  $N(r)$  is identical for different  $\gamma$ 's, as shown by the overlay of the three sets of data plotted as squares in Fig. 3(b). This independence of  $N(r)$  on  $\gamma$  also

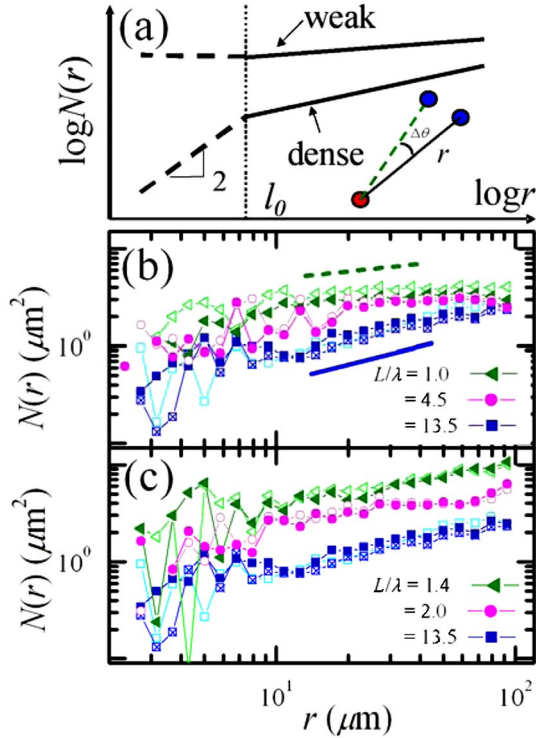


FIG. 3 (color online). (a) Schematic summary of the physical picture described in the text. At  $r < l_0$ , the dense network and weak network exhibit two extreme behaviors of  $N(r)$ , scaling as  $r^2$  and  $r^0$ , respectively. At  $r > l_0$ , the behavior is intermediate between the two extremes. The solid lines indicate the experimentally accessible region. The inset shows schematically the relative position of two particles after  $\gamma$  is applied. The solid line is the actual separation while the dashed line is the separation if the strain were strictly affine. The deviation in angle is  $\Delta\theta$ . (b)  $N(r)$  for  $F$ -actin networks with  $L = 10 \mu\text{m}$ , and different cross-link density,  $c_A = 1 \text{ mg/ml}$ ,  $R = 0.06$  (squares, strain 18%–30%);  $c_A = 0.75 \text{ mg/ml}$ ,  $R = 0.01$  (circles, strain 24%–30%);  $c_A = 0.5 \text{ mg/ml}$ ,  $R = 0.002$  (triangles, strain 23%–28%). The solid line shows  $\sim r^{0.6}$  and the dashed line shows  $\sim r^{0.3}$ . (c)  $N(r)$  for  $F$ -actin networks with fixed cross-link density ( $c_A = 1 \text{ mg/ml}$ ,  $R = 0.06$ ), and different  $L$ ,  $10 \mu\text{m}$  (squares, strain 18%–30%),  $1.6 \mu\text{m}$  (circles, 10%–18%) and  $1.1 \mu\text{m}$  (triangles, 11%–20%). All data are taken at  $25^\circ\text{C}$ .

confirms that our measurements are not influenced by noise or uncertainty in position, which will not increase with  $\gamma$ . Moreover, we estimate that uncertainty due to thermal motion of the particles is about 10 times smaller than what we measure. At shorter  $r$ , however, the smaller number of bead pairs increases the statistical uncertainty. We find  $N(r) \sim r^{0.6}$ , as indicated by the solid line in Fig. 3(b). When the cross-link density is decreased ( $c_A = 0.75 \text{ mg/ml}$ ,  $R = 0.01$ ;  $c_A = 0.5 \text{ mg/ml}$ ,  $R = 0.002$ ), the magnitude of  $N(r)$  increases while the exponent decreases, but the data remain independent of  $\gamma$ , as shown by the circles and triangles in Fig. 3(b).

The parameter  $N(r)$  measures the degree of nonaffinity at a length scale  $r$ . To interpret the  $r$  dependence, we consider the case when  $r$  is smaller than a correlation

length,  $l_0$ . The relative deformation of two points separated by  $r$  along a filament can have two limiting behaviors depending on the filament rigidity. Very rigid filaments or bundles will lead to highly correlated deformations for  $r < l_0 \sim L$ , since the filament will behave like a rod and rotate under shear. The deviation from affine deformation characterized by  $\Delta\theta$  will then be independent of  $r$ , leading to  $N(r) \sim r^2$  for  $r < l_0$ . In contrast, if the two points are not connected by a filament, or if the filament is very flexible, the points will tend to move independently, resulting in  $N(r) \sim r^0$ . However, this behavior will be highly sensitive to the presence of intervening filaments; as a result, we expect large sample-to-sample variations in  $N(r)$  for small separations.

For larger  $r$ , we expect some residual correlations for densely cross-linked networks. We assume this can be roughly approximated by a power law  $N(r) \sim r^\alpha$ , with  $0 < \alpha < 2$  when  $r > l_0$ . As the networks become less dense or more poorly connected, we expect the correlations to be weaker; as a result,  $\alpha$  decreases toward 0. Moreover, due to a smaller energy cost for strain fluctuations in more weakly cross-linked networks, the magnitude of  $N(r)$  will increase with decreasing cross-linking for all  $r$ , as summarized in Fig. 3(a). This is consistent with simulation results [7], which indicate that  $l_0 \approx L$ . While the current simulations [6–9,24] are limited to 2D, the same qualitative behavior is expected in 3D. In our experiments, the smallest  $r$  we can probe is  $\sim 2 \mu\text{m}$ ; smaller  $r$  would require much smaller particles and thus much better resolution than we currently achieve. Nevertheless, the  $r$  dependence of  $N(r)$  we measure at larger  $r$ , as well as the magnitude of  $N(r)$  for networks with different cross-link densities, are entirely consistent with this picture. Specifically, we observe a decrease of  $\alpha$  from 0.6 to 0.3 with decreasing cross-link density.

Decreasing  $L$  should produce much the same effect on  $N(r)$  as decreasing the cross-link density, since there will be fewer cross-links per filament at the same  $R$ . For a fixed cross-link density ( $c_A = 1 \text{ mg/ml}$ ,  $R = 0.06$ ),  $N(r)$  indeed increases as  $L$  decreases from  $10 \mu\text{m}$  to  $1 \mu\text{m}$ , through addition of increasing concentration of gelsolin, as shown in Fig. 3(c), further supporting the theoretical prediction.

To quantify the combined effect of both cross-link density and  $L$  on network connectivity, we use a dimensionless microstructure parameter  $L/\lambda$ , where  $\lambda \sim l_c(l_c/l_b)^{1/3}$ , with  $\lambda$  the distance along a filament over which the deformation is nonaffine [7],  $l_c$  the mean distance between cross-links and  $l_b$  a length of order the filament radius. Thus, the ratio  $L/\lambda$  essentially measures the number of cross-links per filament, which characterizes how strongly connected the network is. Although  $l_c$  is not independently measured, previous studies of the nonlinear properties of actin-scrutin networks have shown that  $l_c \sim c_A^{-1/2} R^{-0.6}$  for unshortened actin filaments [1,25]; we assume that this same dependence also applies upon addition of gelsolin. Using this, we can estimate  $L/\lambda$  up to an unknown pre-

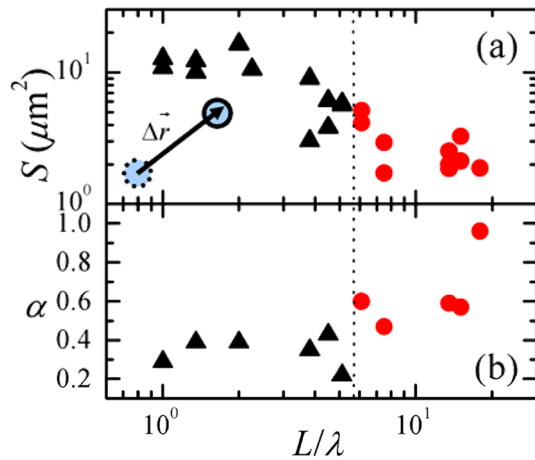


FIG. 4 (color online). Relation of (a) scalar nonaffinity parameter  $S$ , and (b) exponent of  $r$ -dependence of  $N(r)$  to nonlinear rheology for different relative microstructure parameters,  $L/\lambda$ . The stiffening (circles) and weakening (triangles) samples, distinguished by microrheology experiments shown in Fig. 2, are separated by the dotted line. For all samples,  $\gamma$  ranges from 10%–30%. In the inset of (a),  $\Delta\vec{r}$  is defined as the vector connecting the actual position of a single particle after shear (circle) and its position after a strictly affine shear (dotted circle). All data are taken at 25 °C.

factor for the data shown in Figs. 3(b) and 3(c). Since the prefactor is not known, we scale this ratio by its value for the most weakly connected networks ( $c_A = 0.5$  mg/ml,  $R = 0.002$ ). The most strongly connected network has a value of  $L/\lambda$  that is 13.5 times larger. Decreasing either the cross-link density or  $L$  leads to a smaller  $L/\lambda$ , and a concomitant increase in  $N(r)$ .

While  $N(r)$  measures nonaffinity at different  $r$ 's, other measures are possible [26], including a single scalar quantity to facilitate comparison among many samples. It measures the average deviation from affinity,  $S = \langle \Delta\vec{r} \cdot \Delta\vec{r} \rangle / \gamma^2$ , where  $\Delta\vec{r}$  is the deviation of a particle from the affine position after shear, as shown schematically in the inset of Fig. 4(a), and  $\langle \rangle$  denotes averaging over all particles. We observe an increase in  $S$  as the relative  $L/\lambda$  is decreased, as shown in Fig. 4(a). This trend of  $S$  is in excellent agreement with that of  $N(r)$ . Meanwhile, as the sample becomes more nonaffine with decreasing relative  $L/\lambda$ , its nonlinear rheology changes from stiffening (circles) to nonstiffening (triangles), consistent with the entropic stretching origin of stiffening [1,3,5]. In contrast, when the network deforms more nonaffinely, there is no stiffening, since the response is dominated by bending of individual filaments [1,7,8], which is inherently more linear.

We have directly probed the microscopic deformation of  $F$ -actin networks, while simultaneously measuring the nonlinear rheology using microrheology. This technique provides a promising tool to explore the origin of the striking nonlinear properties of  $F$ -actin and other semiflexible polymer networks, and to examine the important

role of various physiological cross-links such as filamin and  $\alpha$ -actinin in this nonlinear response [2,23,27]. While our results are qualitatively consistent with prior 2D simulations and theories [6–9,24], 3D simulations or theory are still necessary for a deeper understanding of cytoskeletal and other biopolymer networks.

We thank T. Stossel, F. Nakamura, and G. Waller. This work was supported by the NSF (Nos. DMR-0602684, CTS-0505929), the Harvard MRSEC (No. DMR-0213805), and the FOM/NWO. G.H.K. was supported by a European Marie Curie Grant (No. FP6-2002-Mobility-6B, No. 8526). The confocal microscope is maintained by the Harvard CNS.

\*Present address: AMOLF, Amsterdam, The Netherlands.

- [1] M.L. Gardel *et al.*, *Science* **304**, 1301 (2004).
- [2] P.A. Janmey *et al.*, *J. Biol. Chem.* **261**, 8357 (1986).
- [3] C. Storm *et al.*, *Nature (London)* **435**, 191 (2005).
- [4] R. Tharmann, M.M.A.E. Claessens, and A.R. Bausch, *Biophys. J.* **90**, 2622 (2006).
- [5] F.C. MacKintosh, J. Kas, and P.A. Janmey, *Phys. Rev. Lett.* **75**, 4425 (1995).
- [6] P.R. Onck *et al.*, *Phys. Rev. Lett.* **95**, 178102 (2005).
- [7] D.A. Head, A.J. Levine, and F.C. MacKintosh, *Phys. Rev. Lett.* **91**, 108102 (2003).
- [8] J. Wilhelm and E. Frey, *Phys. Rev. Lett.* **91**, 108103 (2003).
- [9] D.A. Head, A.J. Levine, and F.C. MacKintosh, *Phys. Rev. E* **68**, 061907 (2003).
- [10] M.L. Gardel *et al.*, *Phys. Rev. Lett.* **93**, 188102 (2004).
- [11] K. Kroy and E. Frey, *Phys. Rev. Lett.* **77**, 306 (1996).
- [12] F.G. Schmidt, F. Ziemann, and E. Sackmann, *Eur. Biophys. J.* **24**, 348 (1996).
- [13] I. Cohen, T.G. Mason, and D.A. Weitz, *Phys. Rev. Lett.* **93**, 046001 (2004).
- [14] L. Tilney, *J. Cell Biol.* **64**, 289 (1975).
- [15] M. Schmid *et al.*, *J. Cell Biol.* **124**, 341 (1994).
- [16] M. Sherman *et al.*, *J. Mol. Biol.* **294**, 139 (1999).
- [17] J.H. Shin *et al.*, *J. Mol. Biol.* **337**, 255 (2004).
- [18] J. Liu *et al.*, *Phys. Rev. Lett.* **96**, 118104 (2006).
- [19] M.F. Schmid *et al.*, *J. Mol. Biol.* **221**, 711 (1991).
- [20] J.H. Shin *et al.*, *J. Cell Biol.* **162**, 1183 (2003).
- [21] See EPAPS Document No. E-PRLTAO-98-035720 for confocal images of actin-scrutin networks. For more information on EPAPS, see <http://www.aip.org/pubservs/epaps.html>.
- [22] J.C. Crocker and D.G. Grier, *J. Colloid Interface Sci.* **179**, 298 (1996).
- [23] M.L. Gardel *et al.*, *Proc. Natl. Acad. Sci. U.S.A.* **103**, 1762 (2006).
- [24] C. Heussinger and E. Frey, *Phys. Rev. Lett.* **96**, 017802 (2006).
- [25] J.H. Shin *et al.*, *Proc. Natl. Acad. Sci. U.S.A.* **101**, 9636 (2004).
- [26] B.A. DiDonna and T.C. Lubensky, *Phys. Rev. E* **72**, 066619 (2005).
- [27] M.L. Gardel *et al.*, *Phys. Rev. Lett.* **96**, 088102 (2006).